

V CIRP Conference on Biomanufacturing

Unconventional milling of zirconia-based bioceramic material with nanosecond pulsed laser

Ponticelli Gennaro Salvatore^{a,*}, Venettacci Simone^a, Tagliaferri Flaviana^b, Trovalusci Federica^c, Genna Silvio^c, Guarino Stefano^a

^aUniversity Niccolò Cusano, Department of Engineering, Via Don Carlo Gnocchi 3, Rome 00166, Italy

^bHochschule Mittweida - University of Applied Sciences, Faculty of Engineering Sciences, Technikumplatz 17, Mittweida 09648, Germany

^cUniversity of Rome Tor Vergata, Department of Enterprise Engineering, Via del Politecnico 1, Rome 00133, Italy

* Corresponding author. Tel.: +39-06-4567-8350; fax: +39-06-4567-8379. E-mail address: gennaro.ponticelli@unicusano.it

Abstract

Fabrication of dental restorations made of zirconia-based biomaterials with enhanced mechanical and tribological properties together with customized surface topography and microstructure for promoting enamel adhesion and cell proliferation while hindering bacterial spreading is a very challenging task to accomplish through conventional machining operations. In fact, traditional milling processes of sintered ceramics are typically labor-intensive, therefore expensive and time-consuming, and these aspects can be further exasperated when microsized features are required. On the other hand, unconventional techniques such as laser milling can represent a suitable solution to produce miniaturized individualized structures on advanced ceramics since it is a non-contact thermal process that ensures the elimination of cutting forces and allows hard and brittle materials to be machined without the need for special equipment which requires high investments and long processing times. In this context, this study aims to investigate the capability of a nanosecond pulsed fiber laser to machine samples made of yttria-stabilized zirconia through a systematic experimental approach in order to identify the most suitable process operational parameters combinations that ensure the obtainment of specific surface topographies while minimizing the machining time. The milling process is carried out by using a 30 W Q-switched Yb:YAG fiber laser by controlling laser beam scan speed, scan strategy and hatch distance and following a multi-level factorial design-based experimentation. The adoption of the laser technology to machine yttria-stabilized zirconia results in a high-repeatable, accurate and time-saving process allowing easy control of the process outcomes.

© 2022 The Authors. Published by Elsevier B.V.

This is an open access article under the CC BY-NC-ND license (<https://creativecommons.org/licenses/by-nc-nd/4.0>)

Peer-review under responsibility of the scientific committee of the V CIRP Conference on Biomanufacturing

Keywords: bioceramic; yttria-stabilized-zirconia; laser milling; fiber laser; surface topography.

1. Introduction

Bioceramics made of zirconium dioxide – or zirconia – have gained widespread consensus among academics and practitioners to replace the commonly adopted titanium for dental restorations [1]. This is thanks to their biocompatibility, mechanical properties, and appearance, having indeed a color that is similar to one of the human teeth [2].

To be eligible for dental prosthesis, the base material must guarantee not only suitable fracture toughness and mechanical

strength [3], but requires also additional characteristics, such as biocompatibility together with antibacterial property [4].

Among zirconium dioxide-based bioceramics, yttria-stabilized zirconia (YSZ) exhibits the best mechanical properties in terms of fracture toughness – K_{IC} up to 12 MPa/m^{1/2} – and flexural strength – up to 2 GPa [5,6]. Moreover, it is biocompatible [7,8] and characterized by antimicrobial activity [9]. Therefore, the material properties of YSZ-based bioceramics make them potential alternatives for dental restorations.

Besides the material properties, both the surface topography and visual aspect of the dental restorations play a critical role [2,10]. In fact, surface roughness is considered one of the main factors affecting friction and wear resistance [11], appearance – both in terms of color [12] and translucency [13] – and cell [14] or bacterial [15] adhesion. In particular, a smooth surface is required when low friction and high wear resistance are desired, while a rough surface could enhance the adhesion strength for any subsequent coating [16]. Moreover, it is worth noting that although a rough surface promotes cell adhesion and proliferation [14], the same can happen for bacteria [17]. However, depending on the characteristic dimensions of asperities and surface topography, the resulting surface wettability further influences both cellular and bacterial growth [18].

In this context, induced surface morphology and topography of YSZ during fabrication and post-processing operations for the realization of dental prosthesis strongly affect the resulting tribological, adhesion and appearance properties of the final product.

Among the common modification methods for zirconia-based bioceramics, e.g. machining, sandblasting, chemical etching, etc., the main drawbacks are low accuracy, low material removal rate and damage of the parts, therefore preventing the fabrication of desired geometries [19]. On the contrary, laser processing appeared as an innovative and potential tool for bulk material removal and efficient and rapid fabrication technique for customization of bioceramics surfaces [2]. In fact, laser processing does not contaminate the surface of the part because the machining tool, which is the laser in this case, does not come into contact with the workpiece [20]. This feature also allows hard or brittle materials to be processed avoiding undesired breakages [21,22]. Moreover, the same laser system can be used for different applications providing high flexibility [23–26].

It is worth highlighting that zirconia, being ceramic, during the interaction with the laser beam, does not have almost any free electron available for the absorption of the energy [2,27]. This means that to induce the ablation mechanism for material removal, a higher energy per unit of incidence area, or fluence, is required [28]. Therefore, only short, or ultrashort pulsed lasers can be adopted. Moreover, YSZ is a thermal insulator [29,30] which in combination with its brittleness makes it more susceptible to thermal shocks. In fact, the thermal gradient induced by the laser-bioceramic interaction could promote thermal cracks initiation deteriorating the final quality of the material. Therefore, the interaction process between the laser beam and the zirconia is critical for material removal, surface quality and mechanical performance, and only an accurate choice of the laser parameters can optimize the result [31].

The present work investigates the laser milling process of zirconium dioxide stabilized with yttria (YSZ) to evaluate the influence of the laser process parameters on the surface roughness and material removal rate. By using a Q-Switched 30 W Yb:YAG fiber laser, scanning speed, number of repetitions and hatching distance were controlled by following a multi-level factorial design. Results were analyzed through the statistical method of ANalysis Of Variance (ANOVA).

Finally, samples' surfaces were visually inspected through scanning electron microscopy to define the resulting quality.

2. Materials and Methods

2.1. Sintered yttria-stabilized zirconia

A commercial sintered zirconia stabilized with yttria (BZC0110M BionZ Crystal, by Bionah srl) was adopted in the present study. The samples were under form of blocks $33 \times 15 \times 13 \text{ mm}^3$ in size. Table 1 shows the main characteristics of the adopted material as declared by the producer.

Table 1. Main characteristics of the YSZ samples as declared by the producer.

Characteristic	Value	Unit
Y ₂ O ₃ content	4÷6	Wt%
Al ₂ O ₃ content	< 1	Wt%
Density	~6	g/cm ³
Flexural Strength	1.2÷1.4	GPa
Vickers Hardness	1250	HV ₁₀
Weibull-module	~15	-
Coefficient of Thermal Expansion	~10 ⁻⁵	K ⁻¹

2.2. Laser processing

Laser milling tests were carried out using a 30 W Q-switched nanosecond pulsed Yb:YAG fiber laser (YLP-RA30-1-50-20-20 by IPG Photonics) with a galvanometric scanning head (by LASIT) equipped with a flat-focusing F-Theta lens (QIOPTIQ, by LINOS). Table 2 shows the detailed characteristics of the laser system.

Table 2. Main characteristics of the laser system.

Characteristic	Value	Unit
Wavelength	1064	nm
Nominal average power	30	W
Maximum pulse energy	1	mJ
Maximum peak power	20	kW
Pulse frequency	30	kHz
Pulse duration	50	ns
Mode TEM	00	-
M ²	1.2÷1.5	-
Focused spot diameter	80	μm
Working area	100×100	mm ²

The laser-bioceramic interaction mode and the resulting volume of ablated material strictly depend on the energy density (L_{Fl}), or fluence, and on the power density (L_{Irr}), or irradiance [27,28], which are defined as functions of pulse energy (E_p), pulse power (P_p), pulse frequency (F_p), and pulse duration (d_p):

$$L_{Fl} = \frac{P}{F_p A_\phi}$$

(1)

$$L_{irr} = \frac{L_{FL}}{d_p} \quad (2)$$

where P is the nominal average power and A_ϕ is the focused laser spot area.

2.3. Methods

Laser milling of 5×5 mm² pockets was carried out by keeping constant the pulse frequency at 30 kHz, to obtain the maximum pulse energy of 1 mJ, a pulse power of 20 kW, and a fluence of ~ 0.2 J/mm². The scanning strategy consisted of four alternating passes at 45° for each repetition. While the scanning speed, the number of repetitions and the hatch distance were controlled by following a multi-level factorial experimental plan developed on the basis of the Design Of Experiment methodology [32,33], as described in Table 3. Each experimental condition was replicated three times. It is worth noting that the process parameters were chosen according to a preliminary investigation aimed at identifying the most influencing factors and their range of application.

Table 3. Multi-level factorial plan: 3 terms of scanning speed \times 2 terms of number or repetitions \times 2 terms of hatch distance = 12 conditions.

Control factor	Level			Unit
Scanning speed (v_L)	350	450	500	mm/s
Number of repetitions (R)	10	20	-	-
Hatch distance (d_H)	40	60	-	μ m

Surface quality was evaluated through roughness measurements and samples' surface inspection. Roughness was quantified through the arithmetic mean surface roughness (R_a) according to the ISO 4287:1997 standard. Measurements were carried out by using a 3D surface profiling system (Talysurf CLI 2000, by Taylor Hobson). For each pocket, three profiles were recorded. The acquired data were elaborated using the software MountainsMap® for surface analysis. Moreover, a scanning electron microscope (SEM Leo SUPRA 35, by ZEISS) was used to verify the quality of the machined pockets.

The machined depth (H_m) was evaluated by using a digital microscope (KH-8700 by Hirox) and used to calculate the material removal rate (MRR):

$$MRR = \frac{H_m A_p \rho}{\tau_m} \quad (3)$$

where A_p is the machined area, ρ the density, τ_m the time needed to mill the pocket.

The ablation mechanism responsible for the removal of the material is strongly influenced by the laser parameters, especially by the pulse duration and the number of incident laser pulses [34,35]. The total number of incident laser pulses (N_p) is given by the product of the number of pulses irradiated along the direction of the laser and the number of scan lines

needed to mill the pocket. The former is calculated by dividing the length of the pocket (L) by the pulse spacing, which is the ratio between the scan speed and the pulse frequency. While the pulse number along the other direction is obtained by dividing the width of the pocket (W) by the hatch distance. Finally, considering the number of times that the laser beam scans the surface, R , the total number of laser pulses can be calculated as follows:

$$N_p = R \frac{L}{v_L / F_p} \frac{W}{d_H} \quad (4)$$

A greater number of pulses interacting with the material results in a greater amount of energy transferred. The subsequent increase of the temperature due to the heat accumulation on the pocket surface enhances the absorption of the laser radiation, therefore the removal of the material is expected to be improved. Table 4 shows the resulting values of N_p obtained for the different experimental scenarios.

Table 4. Number of pulses resulting from different experimental conditions.

Scanning speed, mm/s	Number of repetitions	Hatch distance, μ m	Number of pulses
350	10	40	535,714
350	10	60	357,143
350	20	40	1,071,429
350	20	60	714,286
450	10	40	416,667
450	10	60	277,778
450	20	40	833,333
450	20	60	555,556
550	10	40	340,909
550	10	60	227,273
550	20	40	681,818
550	20	60	454,545

3. Results and Discussion

Experimental results are shown in Fig. 2, while Table 5 reports the statistical results of the ANOVA test, which provides the statistical significance of the control factors (v_L , R , d_H) for the MRR and R_a . It is worth noting that in the latter table the significant effects, i.e. $F > F$ -critical, $p < 0.05$, $\Pi > 3\%$, are highlighted by the bold text. F is the Fisher value, p is the level of probability, and Π is the contribution percentage. The F -critical is 4.28 for one degree of freedom and 3.42 for two degrees of freedom.

The ANOVA results indicate that the most relevant parameter for both response variables, i.e. MRR and R_a , is the laser scanning speed. Moreover, R_a is also affected by the number of repetitions and the interaction between scanning speed and hatch distance. Therefore, for sake of brevity, in the following the discussion will be exclusively focused on the effect of the significant parameters affecting MRR and R_a , i.e. v_L , R and $v_L \times d_H$.

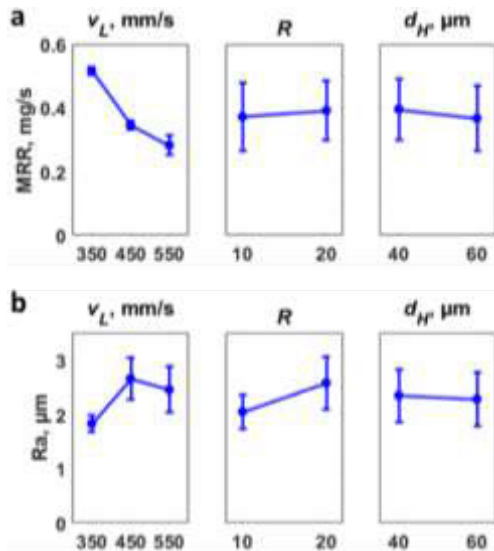


Fig. 1. Experimental results for (a) MRR; (b) R_a . The error bars represent the standard deviation.

Table 5. ANOVA table for MRR and R_a . The significant effects (i.e. $F > F$ -critical, $p < 0.05$, $\Pi > 3\%$) are highlighted by the bold text. The F -critical is 4.28 for one degree of freedom and 3.42 for two degrees of freedom.

Source	MRR			R_a		
	F	p	Π , %	F	p	Π , %
v_L	909.45	0.000	74.55	20.28	0.000	34.15
R	17.71	0.000	0.73	26.61	0.000	22.41
d_H	51.31	0.000	2.10	0.38	0.542	0.32
$v_L \times R$	4.06	0.031	0.33	3.02	0.068	5.09
$v_L \times d_H$	0.72	0.496	0.06	4.68	0.020	7.88
$R \times d_H$	4.96	0.036	0.20	0.32	0.577	0.27
$v_L \times R \times d_H$	6.19	0.007	0.51	0.38	0.685	0.65
Error			0.94			19.36

As shown in Fig. 1a, the lower the scanning speed, the greater the material removal rate, i.e. from an average 0.28 ± 0.03 mg/s at 550 m/s to 0.52 ± 0.01 mg/s at 350 mm/s. In fact, the lower the scanning speed, the longer the time the laser interacts with the material, potentially the higher the average temperature of the machined pocket, the lower the energy needed to reach the melting and the vaporization temperatures. In other words, the number of pulses reaching the pocket is greater (Table 4) and together with a lower level of energy threshold a greater amount of material is removed.

The opposite occurs for the roughness (Fig. 1b). It improves from an average R_a of 2.66 ± 0.39 μm at 450 mm/s to 1.83 ± 0.15 μm at 350 mm/s. In this case, the reason is ascribed to the melting phenomenon, which is restrained due to the lower average temperature the pocket can reach for higher values of scanning speed. Therefore, a lower quantity of particles is ejected from the sample, which tends to re-solidify on the surface (Fig. 2a-b). In this way, the effect peak-valley is more pronounced when the tip of the profilometer meets them during measurements. Moreover, the greater the scanning speed, the lower the surface crack formation due to the thermal shock the samples undergo during the milling process, as confirmed by the presence of

cracks through the droplets of the ejected material, as shown in Fig. 3.

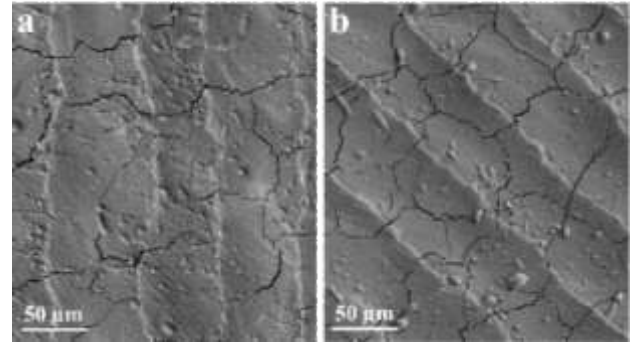


Fig. 2. SEM micrographs of laser milled surfaces at $R = 20$, $d_H = 40$ μm and (a) $v_L = 350$ mm/s or (b) $v_L = 450$ mm/s.

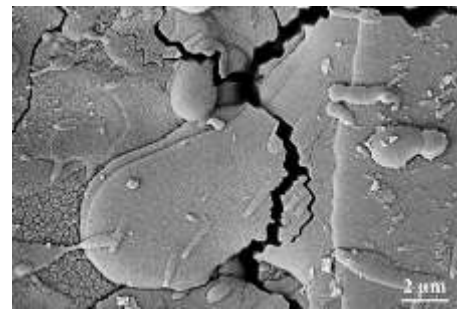


Fig. 3. SEM micrograph of crack propagation of a laser milled surface at $R = 10$, $d_H = 60$ μm and $v_L = 450$ mm/s.

Fig. 1b also highlights that increasing the scanning speed at the highest value here investigated, i.e. 550 mm/s, there is a change of the trend about the roughness. In fact, R_a firstly increases from 1.83 ± 0.15 μm at 350 mm/s to 2.66 ± 0.39 μm at 450 mm/s, but then decreases to 2.45 ± 0.42 μm at 550 mm/s. This effect can be attributed to the interaction between the scanning speed and the hatch distance, as suggested in Table 5 by ANOVA. Increasing the hatch distance together with the scanning speed, the effect peak-valley during roughness measurements is smoothed due to the widening and flattening of the laser scans [36,37]. In fact, the higher the scanning speed and the hatch distance, the lower the number of pulses reaching the surface (Table 4), therefore the lower the total energy transferred to the material, which results in a lower quantity of removed material.

All the surfaces of the milled pockets shown in Fig. 2 are characterized by the presence of cracks covering all the area. This is due to the thermal stresses induced in the sample during the laser milling operation [27,38]. Therefore, the depth of such defects within the material was further investigated. Fig. 4 shows that cracks are limited to the surface and only very few of them infiltrate more in depth, up to 5-10 μm under the surface. However, they are very rare and can be considered as not critical for mechanical strength [38]. But this needs further investigation.

Finally, Fig. 5 shows that the laser processing, within the condition adopted in this work, does not lead to a deep phase transformation, ensuring the preservation of a tetragonal structure.

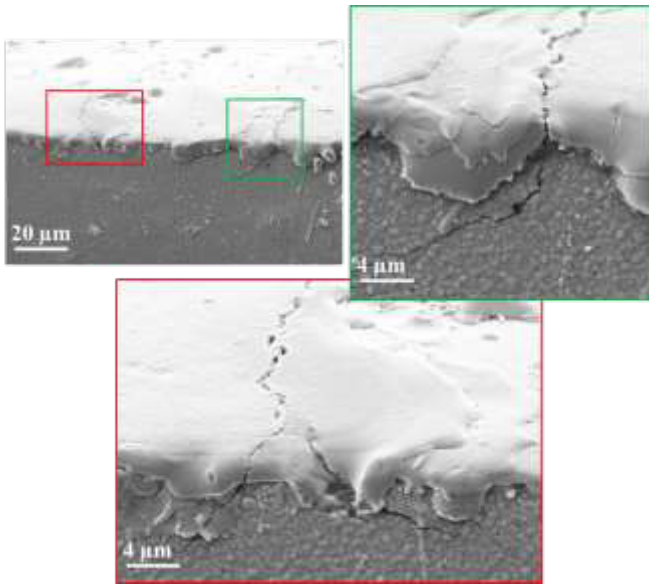


Fig. 4. SEM micrographs of the induced damage due to the laser milling process.

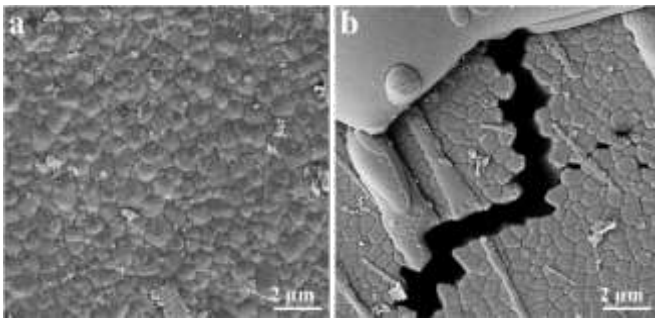


Fig. 5. SEM micrographs of the crystalline structure (a) before and (b) after the laser milling process.

The tribological behaviors between dental restorations and enamel are mainly determined by the mechanical properties and superficial microstructure as well as topography of the restoration material, i.e. zirconia stabilized with yttria in this case. Therefore, observing Fig. 6, in which MRR is plotted as a function of Ra, when a higher roughness value is required, i.e. in order to achieve increased strength with dental porcelain and most importantly good adhesion with dental cement and human dentin or enamel and favoring the osseointegration [2,18], the highest MRR value can be obtained adopting a scanning speed of 450 mm/s, 20 repetitions and 40 μm as hatch distance. Within this condition, a mean Ra of 3.15 μm and a mean MRR of 0.37 mg/s can be obtained (black dot in Fig. 6).

In general, the values of MRR here obtained suggest that the proposed processing method could be only applied to micromachining processes, small batches manufacturing or prototyping, even if compared to picosecond pulsed lasers [39], therefore in line for applications of personalized medicine as in the case of dental prostheses but cheaper than ultrashort pulsed laser systems.

Finally, the existence of cracks and phase transformation raise the question of reliability of the material. The literature [38,39] suggests that such short cracks should not compromise the mechanical strength, however the long-term

effects are worth being studied. Moreover, the surface damage also depends on laser parameters' combination. Therefore, by adequately tuning laser parameters, it is possible to obtain crack-free treatments [40].

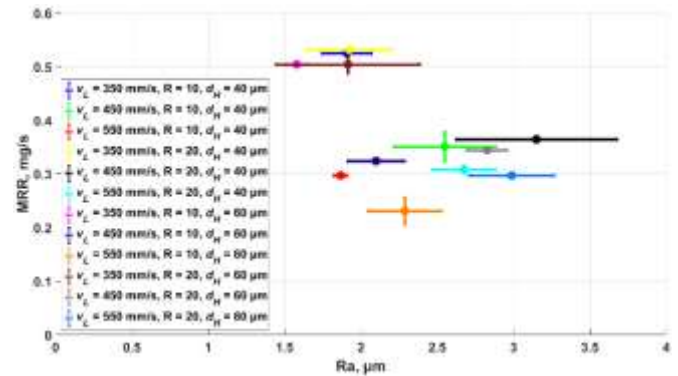


Fig. 6. MRR as a function of Ra for process window identification.

4. Conclusions

The most relevant results of the laser milling of yttria-stabilized zirconia for dental restorations fabrication are listed in the following:

- The lower the scanning speed, the higher the number of pulses, the more enhanced is the absorption phenomena due to the higher surface temperatures, the greater the material removal rate, up to 0.52 ± 0.01 mg/s at 350 mm/s. While the number of repetitions and hatch distance have no significant effect.
- The roughness worsens for increasing values of scanning speed, up to 2.66 ± 0.39 μm at 450 mm/s. This is due to the lower average temperature the pocket can reach for higher values of scanning speed, i.e. lower number of pulses, allowing a smaller quantity of particles to be ejected. These, re-solidifying on the sample surface, enhance the effect peak-valley during measurements, therefore resulting in a rougher surface.
- High material removal rate together with a rough surface are necessary to improve the adhesion of any subsequent coating on the zirconia-based bioceramic substrate. To this end, the experimental findings suggest using the operational parameters' combination given by a scanning speed of 450 mm/s, 20 repetitions and 40 μm as hatch distance.
- In general, the material removal rates obtained are lower than 0.54 mg/s, therefore eligible only for small volume micromachining operations.
- The process guarantees good repeatability, the tendency to maintain the tetragonal structure of the starting material and the induced damage is limited to the near surface region for an extent of about 5-10 μm .

Acknowledgments

CIRTIBS Research Centre of the University of Naples Federico II is gratefully acknowledged for providing the support necessary to develop this research work.

References

- [1] M. Yoshinari, Future prospects of zirconia for oral implants —A review, *Dental Materials Journal*. 39 (2020) 37–45.
- [2] J. Han, F. Zhang, B. van Meerbeek, J. Vleugels, A. Braem, S. Castagne, Laser surface texturing of zirconia-based ceramics for dental applications: A review, *Materials Science and Engineering: C*. 123 (2021) 112034.
- [3] F. Saeed, N. Muhammad, A.S. Khan, F. Sharif, A. Rahim, P. Ahmad, M. Irfan, Prosthodontics dental materials: From conventional to unconventional, *Materials Science and Engineering: C*. 106 (2020).
- [4] Y. Zhu, K. Liu, J. Deng, J. Ye, F. Ai, H. Ouyang, T. Wu, J. Jia, X. Cheng, X. Wang, 3D printed zirconia ceramic hip joint with precise structure and broad-spectrum antibacterial properties, *International Journal of Nanomedicine*. 14 (2019) 5977–5987.
- [5] E. Ferraris, J. Vleugels, Y. Guo, D. Bourell, J.P. Kruth, B. Lauwers, Shaping of engineering ceramics by electro, chemical and physical processes, *CIRP Annals - Manufacturing Technology*. 65 (2016) 761–784.
- [6] M.H.H. Ghaemi, S. Reichert, A. Krupa, M. Sawczak, A. Zykova, K. Lobach, S. Sayenko, Y. Svitlychnyi, Zirconia ceramics with additions of Alumina for advanced tribological and biomedical applications, *Ceramics International*. (2017).
- [7] G. Soon, B. Pinguan-Murphy, K.W. Lai, S.A. Akbar, Review of zirconia-based bioceramic: Surface modification and cellular response, *Ceramics International*. 42 (2016) 12543–12555.
- [8] E. Camposilvan, F.G. Marro, A. Mestra, M. Anglada, Enhanced reliability of yttria-stabilized zirconia for dental applications, *Acta Biomaterialia*. 17 (2015) 36–46.
- [9] M. Khan, M.R. Shaik, S.T. Khan, S.F. Adil, M. Kuniyil, M. Khan, A.A. Al-Warthan, M.R.H. Siddiqui, M. Nawaz Tahir, Enhanced Antimicrobial Activity of Biofunctionalized Zirconia Nanoparticles, *ACS Omega*. 5 (2020) 1987–1996.
- [10] F. Rupp, L. Liang, J. Geis-Gerstorfer, L. Scheideler, F. Hüttig, Surface characteristics of dental implants: A review, *Dental Materials*. 34 (2018) 40–57.
- [11] L. Wang, Y. Liu, W. Si, H. Feng, Y. Tao, Z. Ma, Friction and wear behaviors of dental ceramics against natural tooth enamel, *Journal of the European Ceramic Society*. 32 (2012) 2599–2606.
- [12] L.C. Maciel, C.F.B. Silva, R.H. de Jesus, L.R. da S. Concílio, S.C. Kano, A.A. Xible, Influence of polishing systems on roughness and color change of two dental ceramics, *The Journal of Advanced Prosthodontics*. 11 (2019) 215.
- [13] H.K. Kim, Optical and Mechanical Properties of Highly Translucent Dental Zirconia, *Materials*. 13 (2020) 1–16.
- [14] J. Minguela, M.P. Ginebra, L. Llanes, C. Mas-Moruno, J.J. Roa, Influence of grinding/polishing on the mechanical, phase stability and cell adhesion properties of yttria-stabilized zirconia, *Journal of the European Ceramic Society*. 40 (2020) 4304–4314.
- [15] D.-H. Kang, H. Choi, Y.-J. Yoo, J.-H. Kim, Y.-B. Park, H.-S. Moon, Effect of polishing method on surface roughness and bacterial adhesion of zirconia-porcelain veneer, *Ceramics International*. 43 (2017) 5382–5387.
- [16] S. Guarino, G.S. Ponticelli, O. Giannini, S. Genna, F. Trovalusci, Laser milling of yttria-stabilized zirconia by using a Q-switched Yb:YAG fiber laser: experimental analysis, *International Journal of Advanced Manufacturing Technology*. 94 (2018) 1373–1385.
- [17] S. Roehling, M. Astasov-Frauenhoffer, I. Hauser-Gerspach, O. Braissant, H. Woelfler, T. Waltimo, H. Kniha, M. Gahlert, In Vitro Biofilm Formation on Titanium and Zirconia Implant Surfaces, *Journal of Periodontology*. 88 (2017) 298–307.
- [18] M.F. Kunrath, M.S.G. Monteiro, S. Gupta, R. Hubler, S.D. de Oliveira, Influence of titanium and zirconia modified surfaces for rapid healing on adhesion and biofilm formation of *Staphylococcus epidermidis*, *Archives of Oral Biology*. 117 (2020).
- [19] H.D. Vora, N.B. Dahotre, Laser Machining of Structural Ceramics: An Integrated Experimental and Numerical Approach for Surface Finish, UNT Graduate Exhibition, 2013, Denton, Texas, United States. (2013).
- [20] A. Gisario, M. Barletta, S. Venettacci, F. Veniali, External force-assisted LaserOrigami (LO) bending: Shaping of 3D cubes and edge design of stainless steel chairs, *Journal of Manufacturing Processes*. 18 (2015) 159–166.
- [21] S. Salvatori, G.S. Ponticelli, S. Pettinato, S. Genna, S. Guarino, High-Pressure Sensors Based on Laser-Manufactured Sintered Silicon Carbide, *Applied Sciences*. 10 (2020) 7095.
- [22] A. Orsini, S. Pettinato, D. Baretin, A. Piccardi, G.S. Ponticelli, S. Salvatori, SiC and Diamond Membrane Based Pressure Sensors for Harsh Environments, in: 2021 IEEE International Workshop on Metrology for Industry 4.0 & IoT (MetroInd4.0&IoT), IEEE, 2021: pp. 161–165.
- [23] A. Gisario, M. Barletta, S. Venettacci, F. Veniali, Progress in Tridimensional (3d) Laser Forming of Stainless Steel Sheets, *Lasers in Manufacturing and Materials Processing*. 2 (2015).
- [24] A. Gisario, M. Puopolo, S. Venettacci, F. Veniali, Improvement of thermally sprayed WC-Co/NiCr coatings by surface laser processing, *International Journal of Refractory Metals and Hard Materials*. 52 (2015).
- [25] S. Genna, O. Giannini, S. Guarino, G.S. Ponticelli, F. Tagliaferri, Laser texturing of AISI 304 stainless steel: experimental analysis and genetic algorithm optimisation to control the surface wettability, *International Journal of Advanced Manufacturing Technology*. (2020).
- [26] G.S. Ponticelli, F. Lambiase, C. Leone, S. Genna, Combined Fuzzy and Genetic Algorithm for the Optimisation of Hybrid Composite-Polymer Joints Obtained by Two-Step Laser Joining Process, *Materials*. 13 (2020) 283.
- [27] A.N. Samant, N.B. Dahotre, Laser machining of structural ceramics—A review, *Journal of the European Ceramic Society*. 29 (2009) 969–993.
- [28] C. Leone, S. Genna, F. Tagliaferri, B. Palumbo, M. Dix, Experimental investigation on laser milling of aluminium oxide using a 30W Q-switched Yb:YAG fiber laser, *Optics & Laser Technology*. 76 (2016) 127–137.
- [29] B. Bernard, V. Schick, B. Remy, A. Quet, L. Bianchi, High Temperature Thermal Properties of Columnar Yttria Stabilized Zirconia Thermal Barrier Coating Performed by Suspension Plasma Spraying, *Journal of Physics: Conference Series*. 745 (2016) 032012.
- [30] X.Q.Q. Cao, R. Vassen, D. Stoeber, Ceramic materials for thermal barrier coatings, *Journal of the European Ceramic Society*. 24 (2004) 1–10.
- [31] X. Wang, J.D. Shephard, F.C. Dear, D.P. Hand, Optimized Nanosecond Pulsed Laser Micromachining of Y-TZP Ceramics, *Journal of the American Ceramic Society*. 91 (2008) 391–397.
- [32] D.C. Montgomery, *Design and Analysis of Experiments*, John Wiley, Chichester. (1991).
- [33] D.E. Coleman, D.C. Montgomery, A Systematic Approach to Planning for a Designed Industrial Experiment, *Technometrics*. 35 (1993) 1–12.
- [34] T. Kramer, B. Neuenschwander, B. Jäggi, S. Remund, U. Hunziker, J. Zürcher, Influence of Pulse Bursts on the Specific Removal Rate for Ultra-fast Pulsed Laser Micromachining of Copper, *Physics Procedia*. 83 (2016) 123–134.
- [35] N. Haustrup, G.M. O'Connor, Nanoparticle Generation During Laser Ablation and Laser-Induced Liquefaction, *Physics Procedia*. 12 (2011) 46–53.
- [36] S. Mutluay Unal, S.E. Ozkir, Z. Seyfioglu Polat, S. Guven, H. Asutay, The Effect of Ytterbium-Doped Fiber Laser with Different Parameters on Physical Properties of Zirconia Surface, *Photomedicine and Laser Surgery*. (2016) pho.2016.4176.
- [37] H. Wang, H. Lin, C. Wang, L. Zheng, X. Hu, Laser drilling of structural ceramics - A review, *Journal of the European Ceramic Society*. 37 (2017) 1157–1173.
- [38] E. Roitero, F. Lasserre, J.J. Roa, M. Anglada, F. Mücklich, E. Jiménez-Piqué, Nanosecond-laser patterning of 3Y-TZP: Damage and microstructural changes, *Journal of the European Ceramic Society*. (2017).
- [39] J.P. Parry, J.D. Shephard, D.P. Hand, C. Moorhouse, N. Jones, N. Weston, Laser Micromachining of Zirconia (Y-TZP) Ceramics in the Picosecond Regime and the Impact on Material Strength, *International Journal of Applied Ceramic Technology*. 8 (2011) 163–171.
- [40] Triantafyllidis D, Li L, Stott FH, Crack-free densification of ceramics by laser surface treatment. *Surf Coatings Technol*, 201 (2006) 3163–3173.